Odontology (2019) 107:209–218
https://doi.org/10.1007/s10266-018-0384-z

ORIGINAL ARTICLE

Evaluation of a new tricalcium phosphate for guided bone regeneration: an experimental study in the beagle dog

Mario Pérez-Sayáns[1,2] · Alejandro I. Lorenzo-Pouso[1,2] · Pablo Galindo-Moreno[3] · Fernando Muñoz-Guzón[4] · Antonio González-Cantalapiedra[4] · Mónica López-Peña[4] · Manuel Somoza-Martín[1] · Mercedes Gallas-Torreira[1] · Abel García-García[1,2]

Received: 25 June 2018 / Accepted: 1 August 2018 / Published online: 9 August 2018

Abstract

This study compared the in vivo behavior of two biomaterials, xenograft (Bio-Oss®) and alloplastic tricalcium phosphate (Sil-Oss®), vs a control (no biomaterial) in beagle dogs treated with guided bone regeneration (GBR). Six male adult beagle dogs were included. The third and fourth mandibular premolars and first mandibular molars (3P3, 4P4 and 1M1) on both sides were extracted. After 12 weeks of healing, Straumann implants (3.3 × 8 mm) were placed, performing standardized defects (3.3 × 6 mm) in the vestibular aspect of the alveolar bone. The defects were surgically treated by randomized placement of xenograft (Bio-Oss®), alloplastic tricalcium phosphate (Sil-Oss®) or no biomaterial and covered with a resorbable collagen membrane (BioGide®). After an additional 12-week healing period, the lower jaws were dissected. Total area regenerated in the region of interest, total volume, bone to implant contact in the regenerated area, and volumetric changes were measured through histological, histomorphometrical and microcomputed tomography (microCT) techniques. The negative control group showed bone ingrowth inside the defect, with a partial collapse of the buccal bone. This was not observed in the biomaterial-treated groups. Defects treated with the xenograft showed 51.40% (SD 19.83) newly mineralized tissue, while those treated with alloplastic tricalcium showed 62.54% (SD 11.54) newly mineralized tissue; the control showed 71.52% (SD 6.46). Alloplastic tricalcium phosphate modified with monetite and zinc showed similar features in alveolar regeneration of defects to those treated with the xenograft or conventional GBR, but it showed an ideally higher rate of new mineralized tissue formation and accelerated resorption.

Keywords Guided bone regeneration · Oral implants · Osseous defects · Implantology · Histology

Introduction

Dental implant use has increased considerably in recent years, becoming common practice. This is due in part to developing dental surgical techniques and biomaterials that make this treatment more accessible. A necessary condition for placing dental implants is that a sufficient amount of hard tissues must be available to cover and support the implants [1]. In practice, this condition seldom occurs, and the alveolar bone must be regenerated prior to, or simultaneously with, the implant placement to increase the reabsorbed alveolar crest or treat the localized defects in the alveolar ridge, such as dehiscence or fenestrations [2].

Fenestration-type defects in healthy anatomical situations occur in the 4.1% of modern skulls [3]. Although the prevalence of this hard tissue deficiency increases dramatically with certain biological and technical complications (i.e.,

✉ Mario Pérez-Sayáns
mario.perez@usc.es

1 Oral Medicine, Oral Surgery and Implantology Unit, Faculty of Medicine and Dentistry, Universidade de Santiago de Compostela, Entrerríos s/n, 15782 Santiago de Compostela, Spain

2 Health Research Institute of Santiago de Compostela (IDIS), Santiago de Compostela, Spain

3 Department of Oral Surgery and Implant Dentistry, School of Dentistry, University of Granada, Granada, Spain

4 Department of Veterinary Clinical Sciences, University of Santiago de Compostela, Lugo, Spain

trauma from tooth extraction, periodontal disease, endodontic infections, longitudinal root fractures, etc.) [4]. These osseous defects are mainly treated via guided bone regeneration (GBR). GBR involves the placement of mechanical barriers to protect blood clots and to isolate the bone defect from the connective tissue, thus providing biomaterial space for the osteoproduction phenomena [5]. According to a recent systematic review, GBR leads to high survival and success rates (> 95%) for the implants placed on the regenerated sites [6].

Bone-grafting techniques either with xenografts or allografts still represent a challenge for GBR [7]. Autografts remain as the gold standard for its biological properties, although it has relevant drawbacks such as the need of a surgical harvesting, postoperative morbidity and pain, limited supply and an elevated resorption rate [8].

Anorganic bovine bone (ABB) (Bio-Oss®) is the most studied xenograft in the literature. ABB is highly osteoconductive, allows revascularization of all tissue compartments [9], allows cell recolonization [10], and has high surface protein absorption. In addition, although it presents a very slow resorption rate [11], it allows mineralized tissue to grow relevant to the region where it is placed and non-mineralized tissue of high vascular and cellular richness to form, especially in stromal stem cells [12].

Sil-Oss® (TP) is a tricalcium phosphate-based biomaterial .TP is a Zn-substituted monetite-based scaffold. Monetite is produced by hydrothermal post curing (HTPC). HTPC is based on thermally induced transformation of unstable calcium phosphates phases such as brushite and amorphous calcium phosphate (ACP) into more stable phases such as monetite [13]. The decisive property in monetite's biological behavior is intragranular porosity. Monetite has macropores (< 50 µm), mesopores (50–10 µm), micropores (10 µm–100 nm) and nanopores (> 100 nm), which facilitate osteogenesis, angiogenesis and sustained release of dissolution products (Ca, P, Si, Zn). Compared with xenografts, biomaterials with monetite reabsorb considerably faster [13]. Padilla et al. [14] described TP as a biomaterial composed of Zn-substituted monetite (57 wt%), hydroxyapatite (25 wt%), ACP (11 wt%) and hydrated silica gel (7 wt%), TP was registered under the name of Sil-Oss® (Azurebio, Madrid, MA, Spain). The novelty in this biomaterial's composition is the incorporation of zinc in its formula, which facilitates osteoblastic differentiation while also inhibiting osteoclastic activity [15, 16].

The present study compared the in vivo differential behavior of ABB and TP, in terms of resorption and capacity for regenerating fenestration-type bone defects using GBR.

Materials and methods

Ethics statement

This article was written in accordance with the ARRIVE Guidelines [17]. The experimental protocol was approved by the ethics committee at RofCodina Foundation (Lugo, Spain) and met the relevant regional and European Union requirements (Protocol number: AELUOO1/14/INVMED/OUTROS [04]/FMG/07) for the care and use of research animals. The regional committee for ethics in research approved the trial on 29/10/15 with reference 2015/492.

Study design

This study was designed as a randomized controlled trial with intra-subject control for comparing three treatment procedures. The study was performed in two surgical phases: (a) tooth extraction and (b) implant placement and regeneration of the lateral defect created using guided bone regeneration (three defects per side and animal).

The experimental sites were randomly assigned to one of the three treatment procedures by a randomization list generated by the statistic program Epidat 4.2 (Consellería de Sanidade, Xunta de Galicia, España). Treatment allocation was concealed in sealed envelopes until beginning the GBR procedure.

Animals

Six adult 18- to 19-month-old male beagles (Isoquimen, Barcelona, Spain) with a mean weight of 17.1 kg (range 16.2–19.0) were employed in this study. All animals exhibited fully erupted permanent dentition. The animals were housed in group kennels under controlled environmental conditions (temperature 18–20 °C and relative humidity 50–70%). The dogs were fed granulated dog food moistened with water and had free access to tap water.

Experimental procedures

The animals underwent surgery and were housed in the Animal Experimentation Service Facility at the Veterinary Hospital Rof Codina, Lugo, Spain, from November 2014 to May 2015.

The study began after a 3-week adaption period for the animals. The animals were monitored daily during all experimental procedures by a veterinarian accredited and trained in laboratory animal science.

Surgical procedures

All surgical procedures were performed under general anesthesia in an operating room under sterile conditions, using propofol (3–5 mg/kg/i.v., Propovet, Abbott Laboratories, Kent, UK) and maintained on a concentration of 2.5–4% isoflurane (Isoba-vet, Schering-Plough, Madrid, Spain) and O_2 (100%). The animals were premedicated with medetomidine (0.020 mg/kg/i.m., Esteve, Barcelona, Spain), and their pain was controlled by administering morphine (0.5 mg/kg/i.m., Morfina Braun 2%, B. Braun Medical, Barcelona, Spain). During anesthesia, the animals were continuously monitored by a veterinarian category B or C, controlling electrocardiography, capnography, pulsioxymetry and noninvasive blood pressure.

Atipamezol (0.050 mg/kg/i.m., Esteve, Barcelona, Spain) was administered at the end of the procedure to revert the effects of the medetomidine.

Postoperative pain was controlled with morphine (0.5 mg/kg/i.m., Morfina Braun 2%, B. Braun Medical, Barcelona, Spain) and meloxicam (0.2 mg/kg/s.i.d./p.o.; Metacam, Boehringer Ingelheim, Barcelona, Spain) for 3 days.

During the first postoperative week, the oral mucosa and teeth were disinfected three times weekly using gauze soaked in a 0.12% chlorhexidine solution (Perio-Aid Tratamiento, Dentaid, Barcelona, Spain), followed by a toothbrush and 0.2% chlorhexidine gel (Chlorhexidine Bioadhesive Gel, Lacer, Barcelona, Spain).

Implantation site preparation

The third mandibular premolars and first mandibular molars (3P3, 4P4 and 1M1) on both sides were hemisected and extracted. Subsequently, the alveoli were allowed to heal for 12 weeks, and the animals remained in the veterinary hospital during this time.

Implant placement, defects and GBR procedure

After 12 weeks, the fenestration defects were created in a second experimental phase. For this, vertical releasing incisions were made in the gingiva, and the mucoperiosteal flap was elevated to expose the mandibular bone. The appropriate implant placement sites were chosen, and the bone was prepared per the implant's drilling sequence. Defects 3.3 mm wide and 6.0 mm high were created by drilling the buccal wall of the selected site, exposing the implant surface. The implants (BL NC 3.3 × 8 mm, Straumann, Madrid, Spain) were placed, and the defects were filled with either the test material (TP), the control material (ABB) or left empty (unfilled defect), and in all cases, a Bio-Gide® (Geistlich Bio-Gide®, INIBSA, Barcelona, Spain) membrane was used (Fig. 1). The fenestrations were covered with the membrane, ensuring that they were immobilized. When necessary, they were immobilized by osteosynthesis pins. Mucoperiosteal flaps were then sutured with Supramid 5/0 (Aragó, Barcelona, Spain) obtaining primary closure (Fig. 1). After this surgery, the animals were allowed to heal for 12 weeks. A postoperative antibiotic regimen (cefovecin sodium 8 mg/kg/s.i.d./s.c.; Convenia, Zoetis, Spain) was applied to avoid infection.

Retrieval of specimens

Twelve weeks after implantation and GBR, the animals were humanely killed with an overdose of pentobarbital (60 mg/

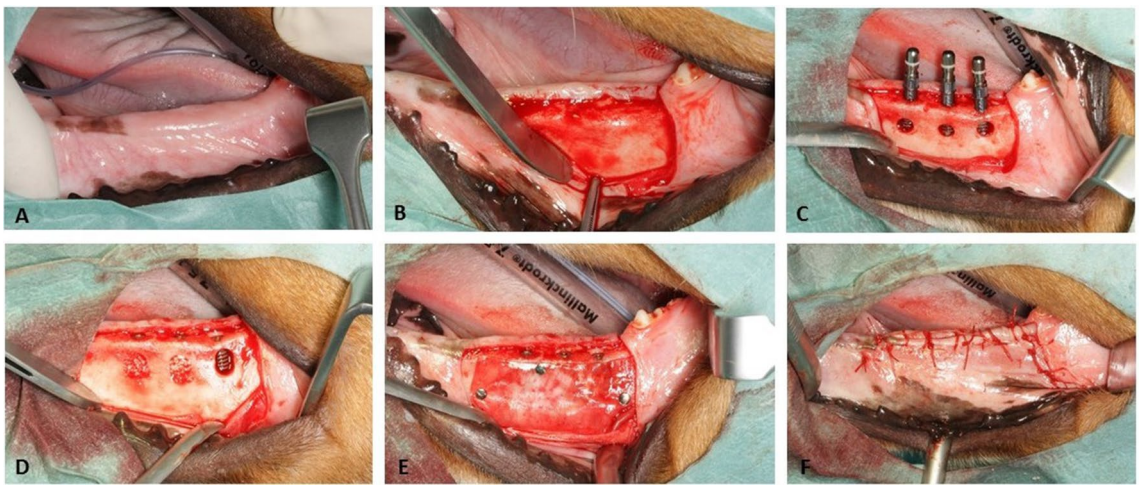

Fig. 1 Intra-operative views. **a** initial, **b** flap design, **c** implant placement and defects generation, **d** defects were implanted with Bio-Oss®, Sil-Oss® or no biomaterial, **e** each defect area was covered with a porcine-derived collagen barrier membrane (BioGide®), **f** flaps were repositioned and primary wound closure was achieved

kg/i.v., Dolethal, Vetoquinol, France) after sedation with medetomidine (0.020 mg/kg/i.m.). Their lower jaws were then dissected and fixed in buffered 10% formaldehyde solution at 4 °C.

MicroCT analysis

Samples were scanned using high-resolution microCT (Skyscan 1172, Bruker microCT NV, Kontich, Belgium). The X-ray source was set at 100 kV and 100 µA with a pixel size of 12 µm and an aluminum/copper filter (Al/Cu). The sample was set on the object stage and scanned with a 360° rotation and images acquired every 0.4°.

After scanning, images were reconstructed based on the Feldkamp algorithm using NRecon software (Bruker microCT NV, Kontich, Belgium) with the same parameters for all samples to allow comparison. The reconstructed images were evaluated using DataViewer software (Bruker microCT NV, Kontich, Belgium). In DataViewer, a volume of interest (VOI) of 5 mm in diameter and 4 mm in apico-coronal length at the center of the implant were selected, avoiding the implant shoulder and apical region.

The data were analyzed using CTAn software (Bruker microCT NV, Kontich, Belgium) using adaptive local thresholding methods. The percentages of bone and material and the ratio of bone volume to total volume (BV/TV) were measured in a section of 20 pixels around the implant. The degree of osseointegration (BIC) was calculated using the method described by Bruker microCT [18].

Histological preparation

Blocks containing the implant and the hard and soft tissues around it were obtained using an oscillating saw and then fixed and identified. The blocks were dehydrated through a graded ethanol series (70–100%) and infiltrated with 4 graded mixtures of ethanol and an infiltrating resin, glycomethacrylate (Technovit 7200®, VLC—Heraus Kulzer GMBH, Werheim, Germany). The last two infiltrations were performed with the pure infiltrating resin under vacuum. The samples were then polymerized, first under low-intensity UV light for 4 h and then under high-intensity UV light for 12 h. Finally, the samples were placed in an oven at 37 °C for 24 h to assure complete polymerization.

From each tissue block, one longitudinal section was prepared in the bucco-lingual direction using a band saw and then mechanically micropolished (ExaktApparatebau, Norderstedt, Germany) using 1200 and 4000 grit silicon carbide papers (Struers, Copenhagen, Denmark) to obtain samples approximately 50 µm thick. The slides were stained with Levai–Laczko stain for histological examination and histomorphometric analysis.

Histomorphometrical analyses

All sections were observed using light microscopy and a PC-based image capture system (BX51, DP71, Olympus Corporation, Japan) and histometrically analyzed. Proportions occupied by bone, biomaterials and soft tissue in the defects were identified from the digital histological images using a pen computer (Cintiq Companion, Wacom, Düsseldorf, Germany), colored (Photoshop, Adobe, San José, CA, USA) and digitally measured using an automated image analysis system (CellSens, Olympus Corporation).

Crestal width and the width of the regenerated area in the defect were measured apically from the shoulder of the implant, at distances of 1 mm for 1–7 mm, for the regenerated vestibular area and the total crestal width. Crestal width of the regenerated area measurements was performed from the buccal implant surface to the buccal outer surface of the neo-formed mineralized tissue.

Two calibrated examiners did the histomorphometrical measurements in duplicate, demonstrating an acceptable intra-examiner variation (Weighted Cohen's Kappa ≈ 0.9) during all the processes.

Statistical analysis

Each implant was taken as a unit of measurement. Qualitative variables were expressed as the frequency and percentage, and quantitative variables were expressed as the mean and standard deviation. To analyze the percentage of regenerated bone relative to the other variables, ANOVA was performed with the Bonferroni test post hoc. The correlations were studied using the Pearson test, considering the values > 0.8 strong, > 0.5 and < 0.8 high, 0.4–0.5 moderate, and < 0.4 low. Based on the most important correlations between the bone percentage relative to the biomaterial and soft tissues, two linear regression models were constructed. The Kruskal–Wallis nonparametric test was used to analyze the crestal width and horizontal regeneration.

Results

Description and general evolution

Animals remained healthy during the experiment, and no adverse effects from the treatment were detected. All implants were osseointegrated. Membranes were histologically visible, and in some cases, presented slight displacement and dehiscence, likely from the animals' chewing.

Two specimens, one negative control and one test group were excluded from the analysis because the material migrated. Five defects were considered failures because the regeneration was incomplete in the defect

area. Four of these were positive controls. Incomplete regeneration of the negative control was caused by excessive buccal placement of the implant. In the positive controls, this appeared to be caused by partial membrane displacement.

In all but three cases, the level of the buccal crest was maintained at the implant shoulder level, and in some cases, the crestal bone partially covered the healing abutment.

Histology and histomorphometry

The defect created was usually refilled with new bone composed of a mixture of newly formed lamellar bone, with regions occupied by progressively maturing bone between them. Bovine particles (positive control group) revealed the fewest degradation signs. The granules were surrounded by mineralized tissue in direct contact, but some granules revealed poor bone growth directly connected to the periosteal region. In these cases, the bone ingrowth was replaced by highly vascularized, dense non-mineralized tissue (Fig. 2b).

In the test group, most of the particles were already degraded upon histological evaluation. This group presented a high regenerative potential, and only one case included a central area colonized by non-mineralized tissue. In the remaining cases (10 of 11), the defect was occupied by mineralized tissue with the same characteristics as the positive control group. The visible particles were completely surrounded by mineralized tissue (Fig. 2a).

The negative control group showed bone ingrowth inside the defect but with a partial collapse of the buccal bone inside it. This was not observed in the particle-treated groups (Fig. 2c).

Analysis of the regenerated bone percentage and its relationship with other variables

Region of interest (ROI) includes the area of the defect surgically created, and was visible thanks to the type of staining used. Levai–Laczkó differentiates the pristine bone of the new or remodelled bone. ROI of the created defect was distinguished by the color change in the bone and the amount and percentage of biomaterial, bone, soft tissues and biomaterial plus bone together (Fig. 3). These were evaluated, considering the latter as the regeneration value. In a complementary manner, bone volume was studied relative to the total volume (BV/TV) and the percentage of bone to implant contact (BIC) and the contralateral bone. The descriptive data are summarized in Tables 1 and 2.

No differences were found relative to the measured area of the defects between the groups (ROI), thus confirming that defect size did not influence the regeneration quantity/quality.

In the defects treated with ABB, the average mineralized tissue was 51.40% (SD 19.83) or 11.34% (SD 7.12) biomaterial and 37.26% (SD 15.60) non-mineralized tissue. In contrast, the defects treated with TP presented an average of 62.54% (SD 11.54) mineralized tissue, 2.27% (SD 4.46) biomaterial and 35.19% (SD 12.23) non-mineralized tissue. The control group showed statistically significant differences ($p = 0.039$) of 71.52% (SD 6.46) mineralized tissue, 0% (SD 0) biomaterial and 28.44% (SD 6.49) non-mineralized tissue. However, because this variable had three categories, applying the Bonferroni post hoc test confirmed that differences existed between the ABB and the control groups ($p = 0.029$).

At 12 weeks, we observed that the percentage of TP remaining in the defect was 5 times less than that of the ABB ($p < 0.0001$). The percentage of non-mineralized tissue did not statistically significantly differ. In the control group,

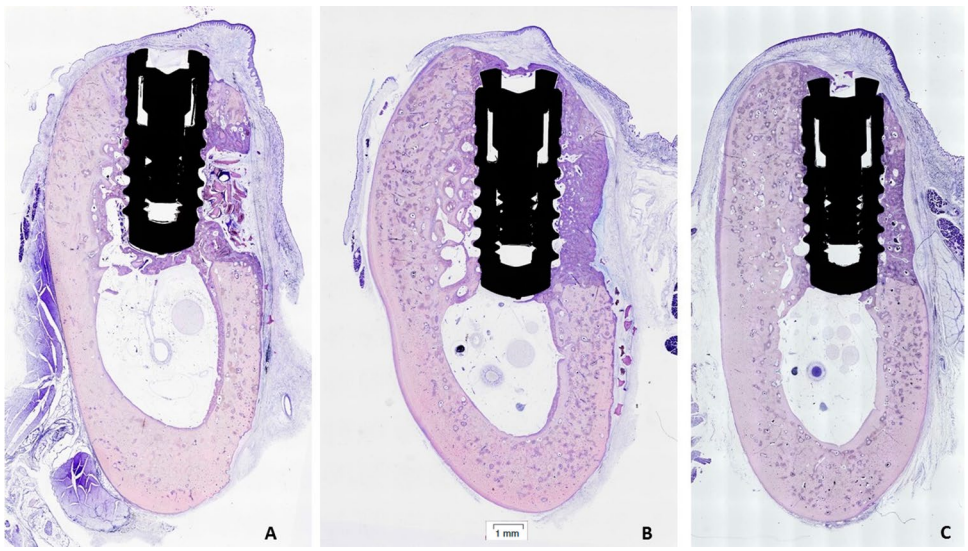

Fig. 2 Buccal–lingual section of implants at 12 weeks showing hard and soft tissues. **a** Bio-oss®, **b** Sil-oss®, **c** non biomaterial. The bars show the magnification

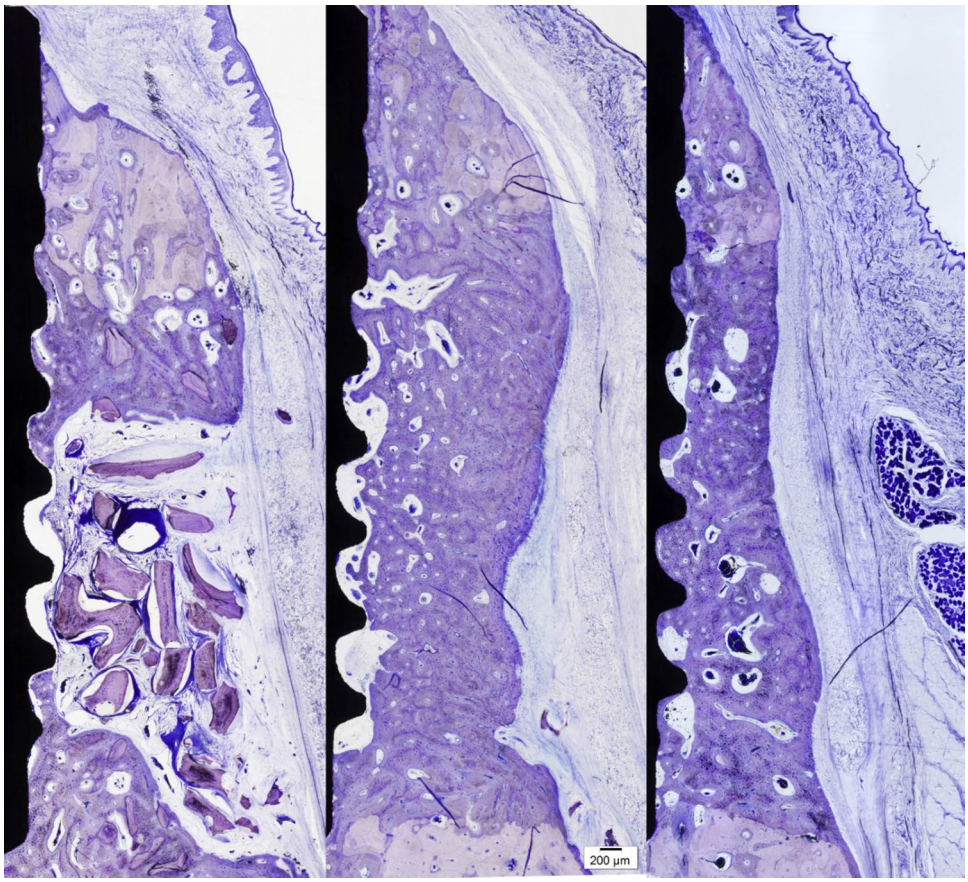

Fig. 3 Buccal section of implants at 12 weeks showing selected regions of interest. **a** Bio-oss®, **b** Sil-oss®, **c** non biomaterial. The bars show the magnification

Table 1 Histomorphometric measurements in each group of the size (mm^2) of the ROI (region of interest) and its proportion (%)

Analyzed structures/tissues	T1 ($n=7$)		T2 ($n=9$)		T3 ($n=11$)		
	mm^2 (SD)	%	mm^2 (SD)	%	mm^2 (SD)	%	*p* value
Total ROI	8.55 (2.41)	100	9.29 (2.32)	100	11.34(7.12)	100	CS: 1.000 CB: 0.663 SB: 1.000 Total: 0.497
Biomaterial	0	0	0.23 (0.45)	2.27	1.23 (0.99)	11.34	CS: 1.000 CB: **0.001** SB: **0.002** Total: **0.000**
Bone	6.14 (0.20)	71.52	5.85 (1.78)	62.64	4.89 (1.68)	51.40	CS: 0.719 CB: **0.029** SB: 0.320 Total: **0.039**
Biomaterial and bone	6.15 (2.03)	71.56	6.09 (1.92)	64.81	6.12 (1.48)	62.74	CS: 0.908 CB: 0.943 SB: 1.000 Total: 0.528
Soft tissues	2.40 (0.72)	28.44	3.20 (1.24)	35.19	3.90 (2.50)	37.26	CS: 0.908 CB: 0.943 SB: 1.000 Total: 0.528

Significant results are reported in bold

C control, *S* Sil-oss®, *B* Bio-oss®, *T1* control (no biomaterial), *T2* tricalcium phosphate (Sil-Oss®), *T3* xenograft (Bio-Oss®)

Table 2 Histomorphometrical analysis in each group validated via quantitative microCT analysis (%)

Measure	*N*	Mean	Standard deviation	*p* value
Bone volume/total volume (BT/TV)				
T1	7	71.88	5.07	CS: 1.000 CB: 1.000 SB: 1.000 Total: 0.457
T2	9	74.46	3.86	
T3	11	71.87	7.59	
Total	27	72.74	5.85	
Bone implant contact microCT (BIC)				
T1	7	72.12	4.05	CS: 1.000 CB: 1.000 SB: 1.000 Total: 0.699
T2	9	73.53	4.13	
T3	11	74.03	4.99	
Total	27	73.37	4.38	
BIC histomorphometry				
T1	6	64.88	16.20	CS: 1.000 CB: 1.000 SB: 1.000 Total: 0.715
T2	8	65.40	16.20	
T3	10	70.82	14.93	
Total	24	67.53	15.24	
BIC native bone				
T1	6	74.69	8.31	CS: 1.000 CB: 1.000 SB: 1.000 Total: 0.896
T2	8	72.78	10.57	
T3	10	75.06	11.73	
Total	24	74.20	10.20	

T1 control (no biomaterial), *T2* tricalcium phosphate (Sil-Oss®), *T3* xenograft (Bio-Oss®), *C* control, *S* Sil-oss®, *B* Bio-oss®

the percentage of mineralized tissue was higher than the groups treated with biomaterials. The regeneration percentage (mineralized tissue + biomaterial) was also greater than in the treated groups, although without statistically significant differences.

The volume of bone obtained for the TP reached an average of 74.46% (SD 3.86), which was higher (but not significantly) than the ABB and control groups, which had values around 71%.

The BIC in the defect measured by histomorphometry showed that the levels were very similar (64–70%), with no significant differences between groups. As an internal control of the histomorphometric measurement, the contralateral BIC was determined in the pristine/native bone, presenting values of 72–75% at 12 weeks for all groups, without statistically significant differences. The BIC in the defect was slightly less than that in the native bone at 12 weeks (7–10% less) for all groups, but without statistically significant differences (Table 2).

We found a strong negative correlation between the percentage of mineralized tissue and that of non-mineralized tissue in the defect [correlation coefficient (CC) − 0.866; $p < 0.0001$] and the biomaterial percentage (CC − 0.528; $p = 0.005$). The ROI and the biomaterial were also moderately correlated with regeneration (CC 0.748, $p < 0.0001$).

Predictive models of regeneration

Based on the most important correlations between the mineralized tissue percentage relative to the biomaterial and non-mineralized tissue, two linear regression models were constructed.

The first model, which was the most powerful, determined that the percentage of mineralized tissue in the defect was explained by 82.8% of the existing non-mineralized tissue ($R^2 = 0.828$; $p < 0.0001$). The model was % mineralized tissue = 100.59–1.17 *x*% non-mineralized tissue (95% CI − 1.395/− 0.954; $p < 0.0001$). For each percent increase in non-mineralized tissue in the defect, the reduction in mineralized tissue varied between − 1.395 and − 0.954%.

The other model determined that the percentage of mineralized tissue in the defect was explained by 45.7% of the existing biomaterial ($R^2 = 0.457$; $p < 0.0001$). The model was % mineralized tissue = 68.68–1.55 *x*% biomaterial (95% CI − 2.243/− 0.854; $p < 0.0001$). Each percent increase in biomaterial in the defect reduced the percentage of mineralized tissue between − 2.24 and − 0.85%.

Analysis of the crestal width and horizontal regeneration

The crestal width in the regenerated zone varied in relation to the biomaterial used, although without statistical differences. Thus, between the first 1–4 mm, (the most coronal area of the implant), regarding the width, control < bio-oss < sill-oss; between 5 and 6 mm, control < TP < ABB and in the most apical zone (7 mm), it was identical to the pattern at 1–4 mm. The Kruskal–Wallis test yielded no statistically significant differences in the vestibular width or total final crestal width as a function of fill type (Table 3).

MicroCT analysis

The BIC measured by microCT presented similar distribution values among all groups (approximately 72–74%), without significant differences. No statistically significant differences were found for the regeneration volume (Fig. 4).

Discussion

This study compared the in vivo behavior of two biomaterials in a vestibular fenestration model in beagles treated by guided bone regeneration. We compared no biomaterial, xenograft (Bio-Oss®) and alloplastic tricalcium phosphate (Sil-Oss®), all isolated by a resorbable membrane.

Table 3 Vestibular width and total bone alveolar width measures expressed in mm stratified by type of biomaterial

	T1 ($n=7$)	T2 ($n=9$)	T3 ($n=11$)	Mean (SD)	p value
Vestibular width mean (SD)	1.51005 (0.23835)	1.73647 (0.63605)	1.83969 (1.15558)	1.732,03 (0.834,22)	0.895
Alveolar bone width mean (SD)	8.38922 (1.11389)	8.88037 (1.20791)	8.99058 (1.11788)	8.78252 (1.130.50)	0.614

T1 control (no biomaterial), *T2* tricalcium phosphate (Sil-Oss®), *T3* xenograft (Bio-Oss®)

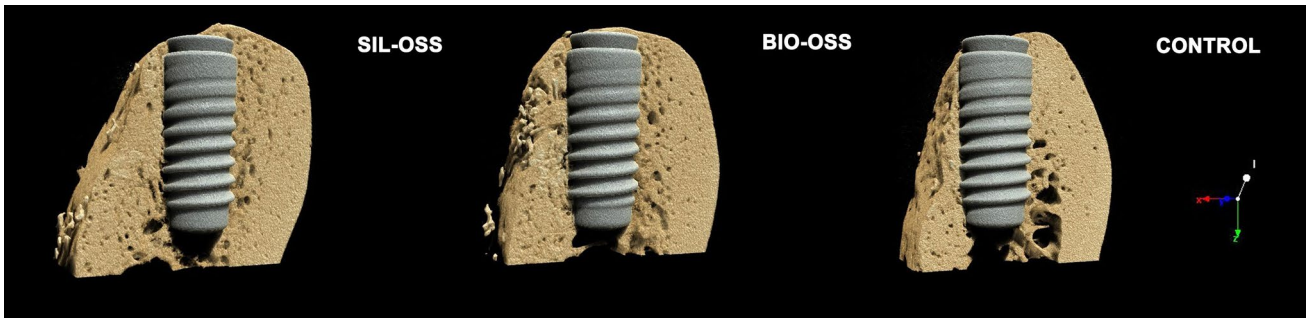

Fig. 4 Three-dimensional reconstruction made by microCT in the different three group

Conceptually, a control defect might be solved with native bone formation, compatible with the normal bone in the treated area. Both block bone substitutes (ABB and TP) after the 12 months of healing maintained their volume and showed minimal absorption. Nonetheless, none graft showed relevant bone formation during this time span.

Different approaches have been analyzed to evaluate these materials. Total area regenerated in ROI, total volume (BV/TV), histomorphometric analysis of the newly formed area, bone to implant contact in the regenerated area (BIC), and volumetric changes were measured. Very few significant differences were found between the biomaterials and the control in regenerating these defects. The authors related this finding to the pivotal role of the intrinsic regenerative capacity of the host which remained equal in the case of ABB and TP. Similar defects in similar areas promote forming similar new pristine bone based on the genetics and function of the area to be replaced. Only chemically modified biomaterials or the use of growth factors can alter this natural bone formation triggering osteoinductive responses [19]. In our study, 71.52% of newly mineralized tissue was found in the controls, while 51.40 and 62.54% of newly mineralized tissue was found in the Bio-Oss® and Sil-Oss®, respectively. Only the control and Bio-Oss® differed significantly in their histomorphometry. This behavior is related to the slower ABB reabsorption [20]. Space occupied by remnant biomaterial cannot be occupied by native tissues. Very little remnant biomaterial was found in the Sil-Oss® group vs. the Bio-Oss® group (2.27 vs 11.34%, respectively). This higher resorption rate allowed more space for the newly mineralized tissue. In our study, this was evidenced by the microCT results. Table 2 shows no differences in bone volume to total volume or bone to implant contact because remnant biomaterial and newly mineralized tissue were dependent between them. Our predictive model certified that 45.7% of the mineralized tissue in the defect was explained by the percentage of existing biomaterial ($R^2=0.457$; $p<0.0001$).The model was % mineralized tissue = 68.68–1.55 x% biomaterial (95% CI − 2.243/− 0.854; $p<0.0001$).

We also found that 82.8% of the mineralized tissue in the defect was explained by the percentage of existing non-mineralized tissue ($R^2=0.828$; $p<0.0001$). The model was % mineralized tissue = 100.59–1.17 x% non-mineralized tissue (95% CI − 1.395/− 0.954; $p<0.0001$). Interestingly, no differences were found in the amount of non-mineralized tissue between the three groups. In human models, quicker biomaterial resorption implied more mineralized tissue, but a poorer quality of non-mineralized tissue, in terms of reparative mesenchymal cells, preosteoblasts and vascularity [21]. In other words, the features of the new non-mineralized tissue conditioned the new bone formation, and both biomaterials showed similar quantities of this tissue compartment to control samples. In this case, accelerated resorption of Sil-Oss® did not appear to have drawbacks. Although they

were not measured in the present study, the cellularity [22] and vascularity [23] promoted by anorganic bone are higher than those of native bone, even higher than those reported in the literature for other biomaterials [24]. This means that the biological activity of ABB is extended over time. In this study, we analyzed our specimens after 12 weeks, and this biomaterial may need more time to express better potential.

Because no significant differences were found between the control and the areas regenerated with Sil-Oss®, this biomaterial effectively promoted bone formation. These results could be due to the modified properties of this tricalcium phosphate alloplastic biomaterial in terms of monetite and zinc presence or because it is quickly degraded, releasing osteoinductive ions into the healing environment. Monetite has excellent osteoinductive properties, similar to those in autogenous bone [13, 25, 26]. Moreover, Zn may play a role in this biomaterial's activity. Some studies using scaffolds loaded with ZnO have shown to exert antibacterial properties [27] as well as increase cell proliferation and wound healing [28]. Osorio and colleagues evidenced the ability of zinc-loaded matrices to promote precipitation of calcium phosphate deposits [29].

The results of the present study show that this monetite-based material has a lower reabsorption rate than other alloplasts, making it more desirable in GBR [13, 30]; however, using zinc in guided bone regeneration has limited evidence. Chou et al. [31] reported in a preclinical in vivo assay that a resorbable membrane composed of zinc and hydroxyapatate showed similar results to a traditional collagen membrane. Regarding the bone dynamics previously described, the addition of zinc to future formulations of filler biomaterials is likely [14, 15].

Two randomized controlled trials (RCTs) have also given insight into the Sil-Oss® osteogenic properties. Flores-Fraile reported the usefulness of TP and Bio-Oss® as biomaterials for alveolar ridge preservation techniques. Both biomaterials showed a similar performance; in this sense, alveolar bone experienced small reduction in width (-0.9 ± 1.3 mm TP vs. -0.6 ± 1.5 mm ABB) and height (-0.1 ± 0.9 mm TP vs. -0.3 ± 0.7 mm ABB) in both experimental groups with no significant results [32]. In other RCT, Kumar et al. studied the efficacy of TP in the treatment of intrabony three wall defects compared to a hydroxyapatite-based scaffold. In this case, TP showed a better clinical performance in relation to hydroxyapatite (HA) in terms of tissue mineralization (25.38% TP vs. 23.73% HA) but no significant differences regarding probing pocket depth and clinical attachment loss at 6 months [33].

The values for the total regenerated area (ROI), vestibular width, and the total width of the regenerated area in our study were similar under all three experimental conditions, thus reinforcing the previous discussion and indicating the suitability of both biomaterials for reproducing and integrum healing of fenestrated areas in a similar manner to native bone.

Within the limitations of the present study, the present Zn-substituted monetite-based scaffold has shown the potential to function as a graft material for periodontal regeneration. Furthermore, the obtained results will have to be validated for clinical applicability.

Funding This study has been partially supported by grants from Ministry of Economy and Competitiveness (Ref. RTC-2014-1731-1). The funders had no role in the study design, data collection and analysis, decision to publish, or in the preparation of the manuscript.

Compliance with ethical standards

Conflict of interest The authors declare that they have no conflict of interest.

References

1. Albrektsson T, Zarb G, Worthington P, Eriksson AR. The long-term efficacy of currently used dental implants: a review and proposed criteria of success. Int J Oral Maxillofac Implants. 1986;1:11–25.
2. Tinti C, Parma-Benfenati S. Clinical classification of bone defects concerning the placement of dental implants. Int J Periodont Restorat Dent. 2003;23:147–55.
3. Merli M, Merli I, Raffaelli E, Pagliaro U, Nastri L, Nieri M. Bone augmentation at implant dehiscences and fenestrations. A systematic review of randomised controlled trials. Eur J Oral Implantol. 2016;9:11–32.
4. Hammerle CHF, Tarnow D. The etiology of hard- and soft-tissue deficiencies at dental implants: a narrative review. J Clin Periodontol. 2018;45(2):267–77.
5. Benic GI, Hammerle CH. Horizontal bone augmentation by means of guided bone regeneration. Periodontol 2000. 2014;66:13–40.
6. Sanz-Sanchez I, Ortiz-Vigon A, Sanz-Martin I, Figuero E, Sanz M. Effectiveness of lateral bone augmentation on the alveolar crest dimension: a systematic review and meta-analysis. J Dent Res. 2015;94:128–42.
7. Yamada M, Egusa H. Current bone substitutes for implant dentistry. J Prosthodont Res. 2018;62:152–61.
8. Miron RJ, Zhang YF. Osteoinduction: a review of old concepts with new standards. J Dent Res. 2012;91:736–44.
9. Galindo-Moreno P, Moreno-Riestra I, Avila G, et al. Effect of anorganic bovine bone to autogenous cortical bone ratio upon bone remodeling patterns following maxillary sinus augmentation. Clin Oral Implants Res. 2011;22:857–64.
10. Galindo-Moreno P, Hernandez-Cortes P, Aneiros-Fernandez J, et al. Morphological evidences of Bio-Oss(R) colonization by CD44-positive cells. Clin Oral Implants Res. 2014;25:366–71.
11. Galindo-Moreno P, Hernandez-Cortes P, Mesa F, et al. Slow resorption of anorganic bovine bone by osteoclasts in maxillary sinus augmentation. Clin Implant Dent Relat Res. 2013;15:858–66.
12. Galindo-Moreno P, de Buitrago JG, Padial-Molina M, Fernandez-Barbero JE, Ata-Ali J, O Valle F. Histopathological comparison of healing after maxillary sinus augmentation using xenograft mixed with autogenous bone versus allograft mixed with autogenous bone. Clin Oral Implants Res. 2018;29:192–201.

13. Torres J, Tamimi F, Alkhraisat MH, et al. Vertical bone augmentation with 3D-synthetic monetite blocks in the rabbit calvaria. J Clin Periodontol. 2011;38:1147–53.
14. Padilla S, de Castro A, Garzón-Gutiérrez A, et al. Novel nanostructured Zn-substituted monetite based biomaterial for bone regeneration. J Nanomed Nanotech. 2015;325:6.
15. Moonga BS, Dempster DW. Zinc is a potent inhibitor of osteoclastic bone resorption in vitro. J Bone Miner Res. 1995;10:453–7.
16. Araujo MG, Liljenberg B, Lindhe J. beta-Tricalcium phosphate in the early phase of socket healing: an experimental study in the dog. Clin Oral Implants Res. 2010;21:445–54.
17. Kilkenny C, Browne W, Cuthill IC, Emerson M, Altman DG, National Centre for the Replacement, Refinement and Reduction of Animals in Research. Animal research: reporting in vivo experiments—the ARRIVE guidelines. J Cereb Blood Flow Metab. 2011;31:991–3.
18. Bruker A. Osteointegration. Analysis of bone around a metal implant (method note No. MN074). 2015. http://www.foa.unesp.br/home/pesquisa/escritorio_de_apoio_a_pesquisa/bruker-micro-ct-academy-2015.pdf. Accessed 17 July 2018.
19. Larsson L, Decker AM, Nibali L, Pilipchuk SP, Berglundh T, Giannobile WV. Regenerative medicine for periodontal and peri-implant diseases. J Dent Res. 2016;95:255–66.
20. Galindo-Moreno P, Leon-Cano A, Ortega-Oller I, Monje A, O'Valle F, Catena A. Marginal bone loss as success criterion in implant dentistry: beyond 2 mm. Clin Oral Implants Res. 2015;26:28–34.
21. Araujo MG, Lindhe J. Ridge alterations following tooth extraction with and without flap elevation: an experimental study in the dog. Clin Oral Implants Res. 2009;20:545–9.
22. Galindo-Moreno P, Moreno-Riestra I, Avila G, et al. Histomorphometric comparison of maxillary pristine bone and composite bone graft biopsies obtained after sinus augmentation. Clin Oral Implants Res. 2010;21:122–8.
23. Galindo-Moreno P, Padial-Molina M, Fernandez-Barbero JE, Mesa F, Rodriguez-Martinez D, O'Valle F. Optimal microvessel density from composite graft of autogenous maxillary cortical bone and anorganic bovine bone in sinus augmentation: influence of clinical variables. Clin Oral Implants Res. 2010;21:221–27.
24. Boeck-Neto RJ, Artese L, Piattelli A, et al. VEGF and MVD expression in sinus augmentation with autologous bone and several graft materials. Oral Dis. 2009;15:148–54.
25. Marino FT, Torres J, Tresguerres I, Jerez LB, Cabarcos EL. Vertical bone augmentation with granulated brushite cement set in glycolic acid. J Biomed Mater Res A. 2007;81:93–102.
26. Karageorgiou V, Kaplan D. Porosity of 3D biomaterial scaffolds and osteogenesis. Biomaterials. 2005;26:5474–91.
27. Augustine R, Dominic EA, Reju I, Kaimal B, Kalarikkal N, Thomas S. Electrospun polycaprolactone membranes incorporated with ZnO nanoparticles as skin substitutes with enhanced fibroblast proliferation and wound healing. RSC Adv. 2014;4:24777–85.
28. Augustine R, Dominic EA, Reju I, Kaimal B, Kalarikkal N, Thomas S. Electrospun poly(epsilon-caprolactone)-based skin substitutes: in vivo evaluation of wound healing and the mechanism of cell proliferation. J Biomed Mater Res B Appl Biomater. 2015;103:1445–54.
29. Osorio R, Alfonso-Rodriguez CA, Osorio E, et al. Novel potential scaffold for periodontal tissue engineering. Clin Oral Investig. 2017;21:2695–707.
30. Tamimi FM, Torres J, Tresguerres I, Clemente C, Lopez-Cabarcos E, Blanco LJ. Bone augmentation in rabbit calvariae: comparative study between Bio-Oss and a novel beta-TCP/DCPD granulate. J Clin Periodontol. 2006;33:922–8.
31. Chou J, Komuro M, Hao J, et al. Bioresorbable zinc hydroxyapatite guided bone regeneration membrane for bone regeneration. Clin Oral Implants Res. 2016;27:354–60.
32. Flores-Fraile J [Safety and efficacy of the new biomaterial Sil-Oss in the regeneration of post-extraction alveolar ridge. A randomized comparative clinical trial] Universidad de Salamanca. 2016. https://gredos.usal.es/jspui/handle/10366/132812. Accessed 17 July 2018.
33. Kumar-Deshoju A, Viswa-Chandra R, Amarender-Reddy A, Harish-Reddy B, Nagarajan S, Naveen A. Efficacy of a novel Zn-substituted monetite-based scaffold in the treatment of periodontal osseous. J Intern Acad Periodontol. 2017;19:2–9.